

# Preparation and Corrosion Resistance of ZnO Films under Different Annealing Temperatures and Their Resistive Switching Behaviours

Fengzhu Zhao<sup>1,2</sup>, Qiushi Li<sup>3</sup>, Jihui Wang<sup>1,2,\*</sup>, Wenbin, Hu<sup>2</sup>

<sup>1</sup> State Key Laboratory of Hydraulic Engineering Simulation and Safety, Tianjin University, Tianjin 300350, P R China

<sup>2</sup> School of Materials Science and Engineering, Tianjin University, Tianjin 300350, P R China

<sup>3</sup> Tianjin Port Engineering Institute Co., Ltd., CCCC First Harbor Engineering Co., Ltd., Tianjin 300222, P R China

\*E-mail: [jhwang@tju.edu.cn](mailto:jhwang@tju.edu.cn)

Received: 21 February 2021 / Accepted: 9 April 2021 / Published: 30 April 2021

---

ZnO resistive switching films were deposited on 304 stainless steel specimens using the sol-gel method under different annealing temperatures. The surface morphology, structure and composition of the ZnO films were characterized by scanning electron microscopy, energy dispersive spectroscopy, and Fourier transform infrared spectroscopy. The semiconductor properties and carrier content of the films were determined by the Mott-Schottky curve, X-ray photoelectron spectroscopy and electron spin resonance techniques, and the corrosion resistance of the films was measured by the polarization curve and electrochemical impedance spectroscopy. The experimental results showed that each prepared film was an *n*-type semiconductor with oxygen vacancies, and the grain size and concentration of the oxygen vacancies in the films increased with increasing annealing temperature. With increasing annealing temperature, the corrosion resistance of the ZnO films first increased and then decreased with the largest corrosion resistance at an annealing temperature of 400°C. By applying a negative polarization treatment, the concentration of oxygen vacancies and the corrosion resistance of the films could be restored to their original states, and the corrosion resistance of the films could be improved with prolonged immersion time due to the combination of oxygen vacancies in the films with oxygen atoms in the solution.

---

**Keywords:** ZnO film, corrosion resistance, resistive switching behaviour, annealing temperature, oxygen vacancy

## 1. INTRODUCTION

Surface coating is a popular technology for improving the corrosion resistance of steels because of its advantages of a good protection effect and lower cost. Traditionally, surface coatings are mainly

divided into organic coatings and inorganic coatings [1]. Among these protective coatings, organic coatings are widely applied due to their simple preparation process, whereas there are various defects, such as pores, bubbles and gaps, in organic coatings, which can easily lead to peeling or failure of the coating [2-4]. Inorganic coatings also have higher protection effects in industrial fields due to their compact structure, good bonding force, and stable physical and chemical properties [5]. However, inorganic coatings can only act as physical barriers in corrosion protection, and a corrosive solution could be easily diffused to the steel surface by coating defects. Therefore, it is necessary to develop a new type of coating with a stable structure, simple preparation and long service life.

As a nontoxic and low-cost inorganic ceramic material, zinc oxide (ZnO) has the advantages of excellent thermal stability, a compact structure and a simple preparation process [6, 7] and is widely applied as a coating or coating additive for steel corrosion protection. Kamburova et al. [8] investigated whether the corrosion resistance of polymeric coatings could be improved by compounding ZnO nanoparticles. ZnO films, ZnO composite films and ZnO-doped films have been deposited on steel surfaces, and the corrosion resistance of steels was obviously enhanced [9-12]. Moreover, a ZnO film is a semiconductor and can be used as a resistive switching film due to its crystal structure and vacancy defects [13]. The oxygen vacancies in the ZnO film could diffuse, disappear or be generated by applying an external voltage, which would lead to resistance changes in zinc oxide [14]. Because of this characteristic, the corrosion resistance of a ZnO film could be improved by the combination of oxygen vacancies in the film with oxygen atoms in the environment, whereby the service life of the film would be prolonged [14, 15].

ZnO films are usually prepared by sol-gel, electrochemical deposition and radio frequency magnetron sputtering methods [16-18]. Among these methods, the sol-gel method is a simple and easily available technology [19, 20]. Therefore, in this work, a ZnO resistive switching film was prepared on a steel surface by using the sol-gel method under different annealing temperatures. The surface morphology, composition and structure of ZnO resistive switching films were observed and determined by scanning electron microscopy (SEM), energy-dispersive X-ray spectroscopy (EDS), and X-ray diffraction (XRD). The semiconductor behaviour, carrier concentration and corrosion resistance of the film were determined by the Mott-Schottky curve, X-ray photoelectron spectroscopy (XPS), electron spin resonance (ESR) spectra, polarization curves and electrochemical impedance spectroscopy (EIS) techniques. The resistance switching behaviour of the film was investigated by immersion and polarization tests. Based on these experimental results, the influence of the annealing temperature on the structure and corrosion resistance of ZnO film was discussed, and then the resistance switching process and protection mechanism of the film were proposed.

## 2. EXPERIMENTAL

### 2.1 Materials

304 stainless steel samples with compositions of 0.05 wt.% C, 0.36 wt.% Si, 1.52 wt.% Mn, 9.32 wt.% Ni, 19.51 wt.% Cr and balanced Fe were used as the substrates of the ZnO resistive

switching film. A stainless steel specimen with the size of 15 mm×15 mm×3 mm was cut from 304 stainless steel plates. Then, the specimen was ground by water sandpapers up to 2000# with subsequent polishing of 1 μm of diamond paste. After immersion in absolute ethanol and cleaning with an ultrasonic cleaner for 10-20 minutes, the specimens were dried and stored in a dry environment for later use.

## 2.2 Preparation

ZnO resistive switching film was prepared by the sol-gel method according to the following steps. First, 13.17 g of Zn (CH<sub>3</sub>COO)<sub>2</sub>·2H<sub>2</sub>O was dissolved in 100 ml of 2-methoxyethanol. Then, ethanolamine with the same molar amount as Zn (CH<sub>3</sub>COO)<sub>2</sub>·2H<sub>2</sub>O (3.66 ml) was added to the above solution. After the mixed solution was stirred at room temperature using a magnetic stirrer for 12 hours, a stable 0.6 mol/L zinc acetate sol was obtained after incubation at 30°C for more than 24 hours.

Then, the stable zinc acetate sol solution was dropped on the steel surface by using the spin-coating method at 1800 rpm for 15 s. After drying at 130°C for 15 min, a precoated film with 12 layers was obtained. After annealing at 350°C, 400°C, 450°C and 500°C for 1 hour in a furnace with an atmosphere of nitrogen, ZnO resistive switching films were obtained.

Due to the properties of ZnO films under different annealing temperatures, blank stainless steel was treated by drying at 130°C for 15 min.

## 2.3 Characterization

The surface morphology of ZnO films under different annealing temperatures was observed by scanning electron microscopy, and the element compositions of the films were measured by affiliated energy dispersive spectroscopy.

The crystal structure of the ZnO film was examined by grazing incidence from 20° to 80° with a scanning speed of 2°/min, and the interplanar spacing and crystal grain size of ZnO films were calculated by the MID jade6 software. The chemical bond information of the ZnO film was determined by Fourier transform infrared spectrometry (FT-IR) at wavenumbers ranging from 4000 cm<sup>-1</sup> to 400 cm<sup>-1</sup>.

The concentration of oxygen vacancies in the ZnO films was analysed by electron spin resonance techniques with a microwave frequency of 9.22 GHz and by X-ray photoelectron spectroscopy with the binding energy calibration of C1 s at 284.8 eV.

## 2.4 Electrochemical tests

The electrochemical performance of ZnO resistive switching films in a 3.5% NaCl solution was carried out at room temperature on an Autolab 302N electrochemical workstation by using a traditional three-electrode electrolytic cell. A ZnO film with an exposure area of 1 cm<sup>2</sup> was used as the working

electrode, while a Ag/AgCl electrode and platinum plate were used as the reference electrode and counter electrode, respectively.

The Mott-Schottky curve of the film was measured under an AC voltage amplitude of 0.01 V and a frequency of 1000 Hz in the potential range from -0.8 V to 0.8 V. The carrier density in the film can be calculated by the Mott-Schottky equation as follows [21]:

$$1/C^2 = \left(2/\varepsilon\varepsilon_0eN_d\right) [E - E_{fb} - (KT/e)] \quad (1)$$

where  $\varepsilon$  is the relative permittivity of the semiconductor film,  $\varepsilon_0$  is the vacuum permittivity ( $8.85 \times 10^{-14}$  F/cm),  $e$  is the quantity of elementary charge,  $N_d$  is the donor carrier density,  $E_{fb}$  is the flat band potential,  $K$  is the Boltzmann constant ( $13.8 \times 10^{-23}$  J/K) and  $T$  is the absolute temperature.

Electrochemical impedance spectroscopy (EIS) of the film was carried out at OCP in the frequency range from 100 kHz to 0.01 Hz with an AC voltage amplitude of 0.01 V. After the tests, the ZsimpWin software was applied to fit the EIS results by the given equivalent circuit. The protection efficiency of the ZnO resistive switching films in a 3.5% NaCl solution was calculated by the following equation:

$$\eta = \left[ (R_{total}' - R_{total}) / R_{total}' \right] \times 100\% \quad (2)$$

where  $\eta$  is the protection efficiency and  $R_{total}' (=R_f + R_{ct})$  is the polarization resistance of the ZnO resistive switching films in a 3.5 wt % NaCl solution. In addition,  $R_{total}' (=R_{ct})$  is the charge transfer resistance of 304 stainless steel in a 3.5 wt % NaCl solution.

### 2.5 Immersion test

To explore the corrosion resistance evolution of the ZnO film, the ZnO film annealed at 400°C was immersed in a 3.5 wt % NaCl solution for 16 hours, and the EIS spectrum of the film was measured during the immersion test. The surface morphology and composition of the ZnO film before and after immersion were characterized by scanning electron microscopy and affiliated energy dispersive spectroscopy. Furthermore, the oxygen vacancy concentration in the ZnO film was determined by X-ray photoelectron spectroscopy and Mott-Schottky curves at different immersion times.

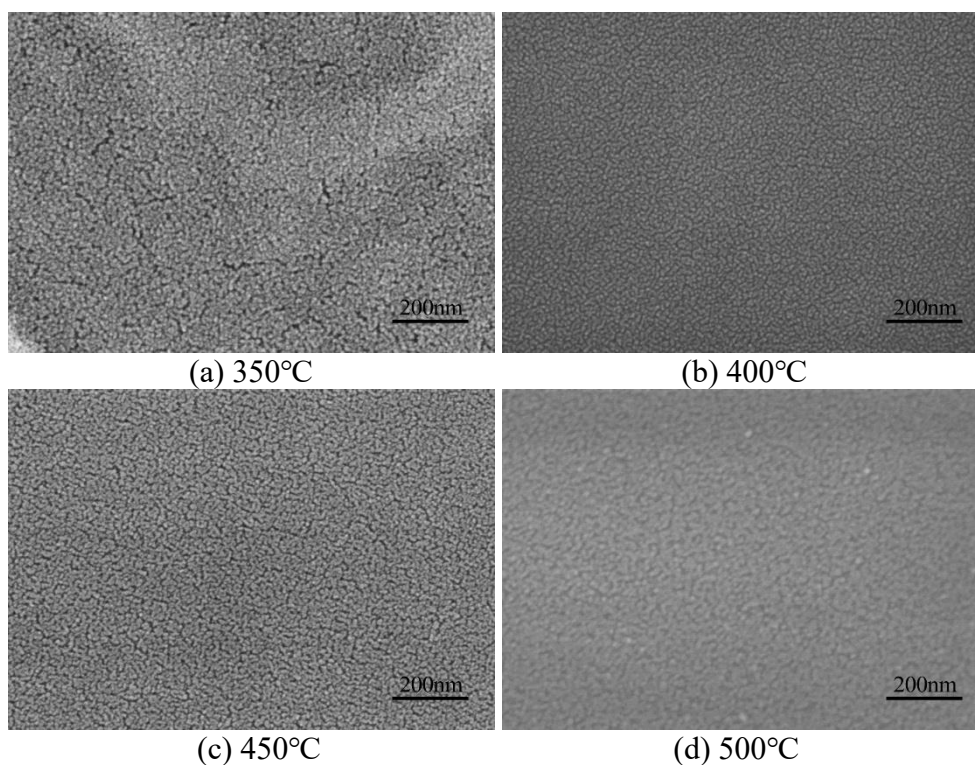
### 2.6 Resistive switching test

To verify the resistance switching behaviour, the ZnO film was first immersed in a 3.5 wt% NaCl solution for four hours, and then the corroded film was transferred to deionized water and polarized for 15 minutes under a voltage of -0.6 V. Next, the polarization-treated specimen was immersed in a 3.5% NaCl solution again, and this immersion-polarization process was repeated three times. During this immersion-polarization process, the EIS spectrum and oxygen vacancy concentration in the ZnO film were also measured in every stage.

### 3. RESULTS

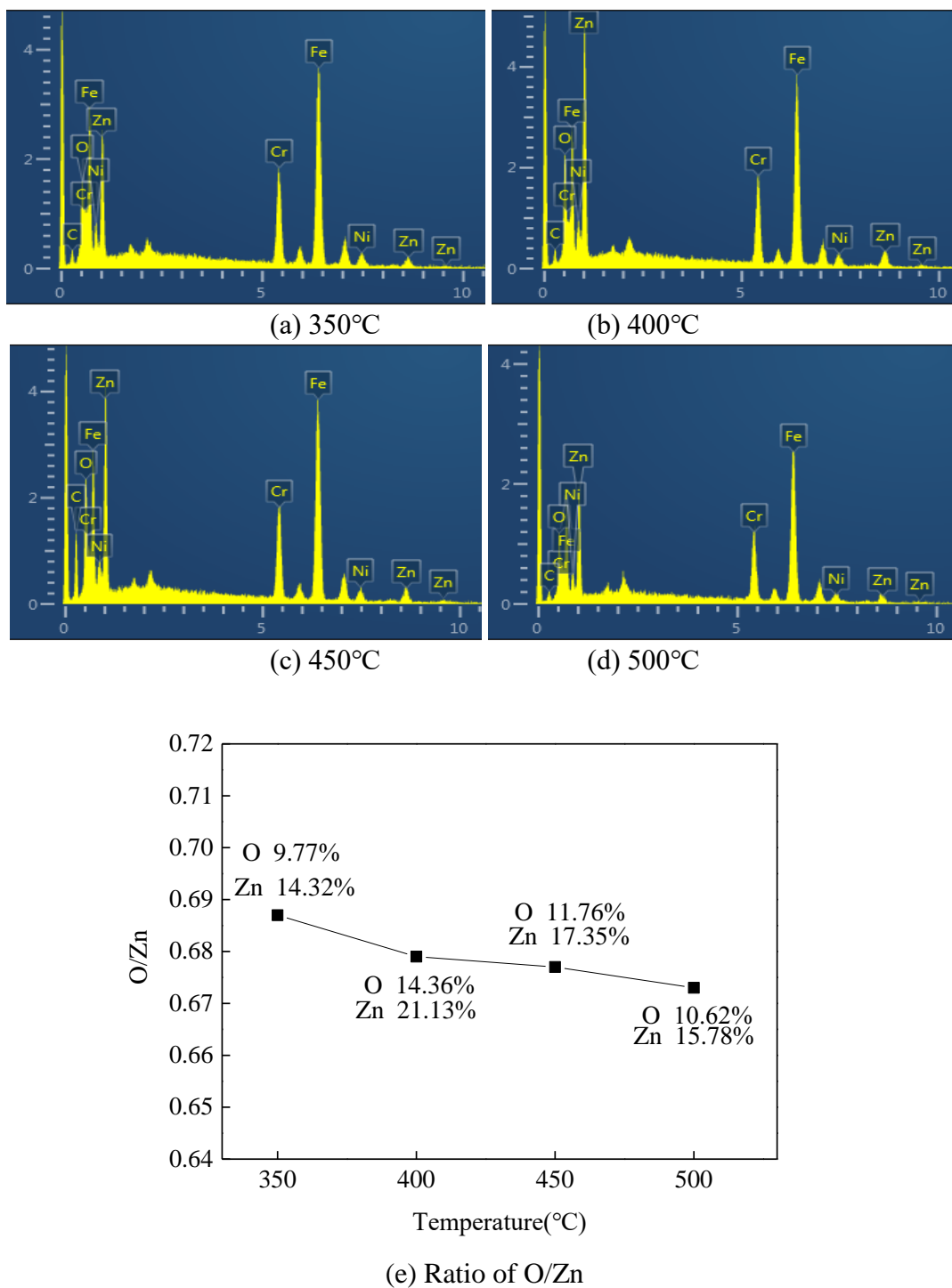
#### 3.1 Morphology and composition

Fig. 1 shows the surface morphology of ZnO films under different annealing temperatures. Under an annealing temperature of 350°C, the ZnO film has a smooth surface with small grains and many pores. When the annealing temperature was increased to 400°C and 450°C, ZnO films were on a homogeneous surface with a slightly larger grain size and almost no pores in the film. With the annealing temperature increasing to 500°C, the grain size of the film is enhanced, and there are more pores in the film.



**Figure 1.** Surface morphologies of ZnO films prepared under different annealing temperatures ( $\times 100000$ )

The EDS spectrum and ratio of O/Zn of ZnO films under different annealing temperatures are shown in Fig. 2. It can be observed that there are Zn, O, Fe, Cr, Ni, O and C elements in the ZnO films, and the Fe, Cr, Ni and O elements are from the substrate of stainless steel, whereas the Zn and O elements originate from the ZnO film. By calculation, the ratio of O/Zn for the ZnO film was between 0.67-0.69, which is less than 1. The ratio of O/Zn for the ZnO film decreased with increasing annealing temperature (Fig. 2e). All of these results mean that there were oxygen vacancies in the ZnO film and that the concentration of oxygen vacancies should increase with increasing annealing temperature.



**Figure 2.** EDS spectra and ratios of O/Zn of ZnO films under different annealing temperatures

### 3.2 Phase structure

Fig. 3 shows the XRD patterns of the 304 SS substrate and ZnO films under different annealing temperatures. In the XRD spectrum of the 304 SS substrate, the diffraction peaks at 43.66°, 50.86° and 74.84° correspond to the (111), (200) and (220) planes of  $\gamma$ -austenite, and the diffraction peak at 44.62° belongs to the (110) plane of  $\alpha$ -ferrite, which indicates that 304 stainless steel is composed of  $\gamma$

and  $\alpha$  phases. In the XRD spectrum of the ZnO film at 350°C, in addition to the diffraction peaks of the  $\gamma$  and  $\alpha$  phases at 43.66°, 50.86°, 74.84° and 44.62°, diffraction peaks at 31.62°, 34.33° and 36.16° were observed that belonged to the (100), (002), and (101) crystal planes of the ZnO hexagonal structure, respectively. When we increased the annealing temperature to 400°C, 450°C and 500°C, the diffraction peaks in the XRD spectrum of ZnO films were almost the same as those at 350°C, which means that the annealing temperature had almost no effect on the crystal structure of the ZnO film.

By calculation, the plane spacings and grain sizes of ZnO films under different annealing temperatures are shown in Table 1. With increasing annealing temperature, the crystal spacing of the (002) plane remained unchanged, but the grain size of the ZnO film increased gradually [22], which is consistent with the surface morphology of the ZnO films in Fig. 1.

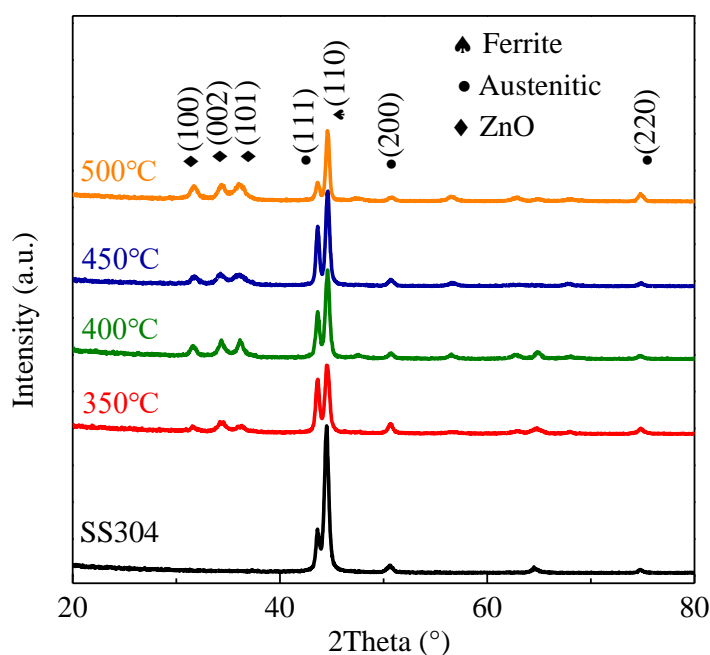


**Figure 3.** XRD pattern of the 304 SS substrate and ZnO films under different annealing temperatures

**Table 1.** Calculation plane spacings and grain sizes of ZnO films under different annealing temperatures

Annealing temperature (°C)	Lattice index	2Theta (°)	Interplanar spacing (nm)	Grain size (nm)
350	(002)	34.335	0.262	4.413
400	(002)	34.307	0.262	5.024
450	(002)	34.361	0.262	5.203
500	(002)	34.342	0.262	6.358

### 3.3 FT-IR spectrum

Fig. 4 shows the FT-IR spectra of ZnO films under different annealing temperatures. In the spectrum of ZnO films at 350°C, the absorption peak at 3432  $\text{cm}^{-1}$  is attributed to the stretching vibration of O-H bonds, which is related to the moisture in the environment. The absorption peak at 1382  $\text{cm}^{-1}$  is assigned to the stretching vibration of the C-H group from glycol methyl ether, which was used as the sol solvent, and the peak at 1604  $\text{cm}^{-1}$  corresponds to the stretching vibration of N-H from the ethanolamine that was used as the sol stabilizer [23-25]. In addition, the absorption peak at 472  $\text{cm}^{-1}$  is related to the stretching vibration of the Zn-O group, which belonged to the ZnO film [23, 26].

When we increased the annealing temperature to 400°C, 450°C and 500°C, the absorption peaks at 472  $\text{cm}^{-1}$ , 1382  $\text{cm}^{-1}$ , 1604  $\text{cm}^{-1}$  and 3432  $\text{cm}^{-1}$  still existed, but the peak intensities of the absorption peaks at 1382  $\text{cm}^{-1}$  and 1604  $\text{cm}^{-1}$  gradually decreased. All of these results show that the functional groups of the ZnO film remained almost unchanged.

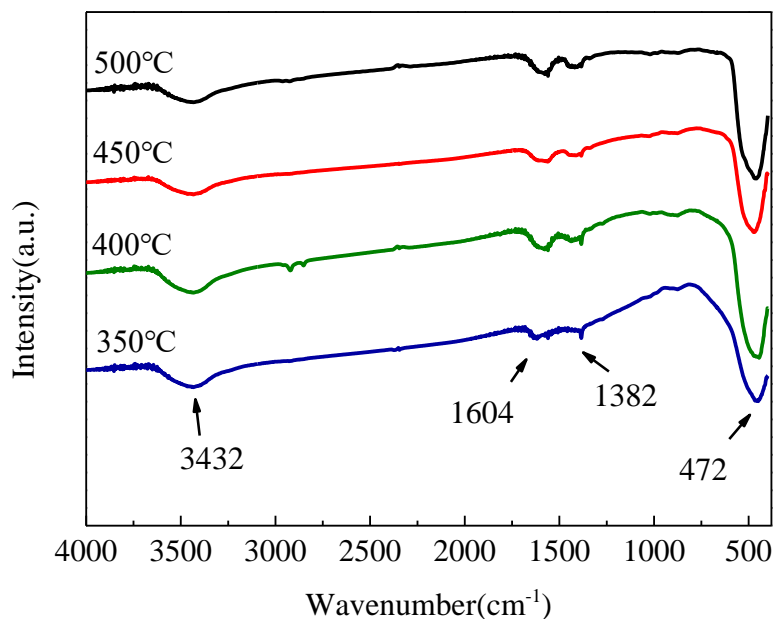


**Figure 4.** FT-IR spectra of ZnO films under different annealing temperatures

### 3.4 ESR spectrum

The ESR spectra of ZnO films under different annealing temperatures are shown in Fig. 5. In the spectrum of ZnO films at 350°C, a sharp signal appeared at 330 mT, which was caused by the positive monovalent oxygen vacancy ( $\text{V}_{\text{O}}^+$ ) defect in the film [27]. When we increased the annealing temperature to 400°C, 450°C and 500°C, a sharp signal of oxygen vacancies was still observed, but the peak intensity of the signal decreased with increasing annealing temperature. Hence, the content of oxygen vacancies in the ZnO film is reduced with increasing annealing temperature, which is consistent with the EDS spectrum in Fig. 2e.

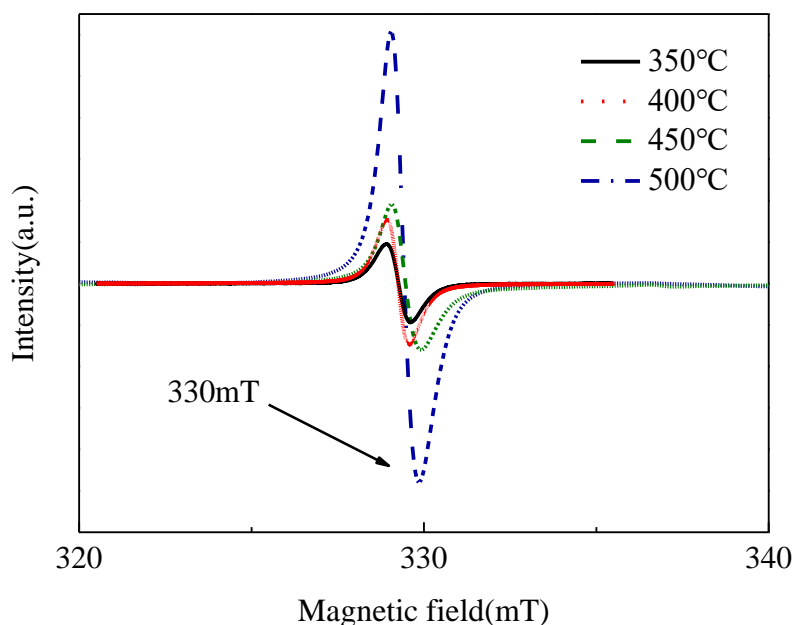
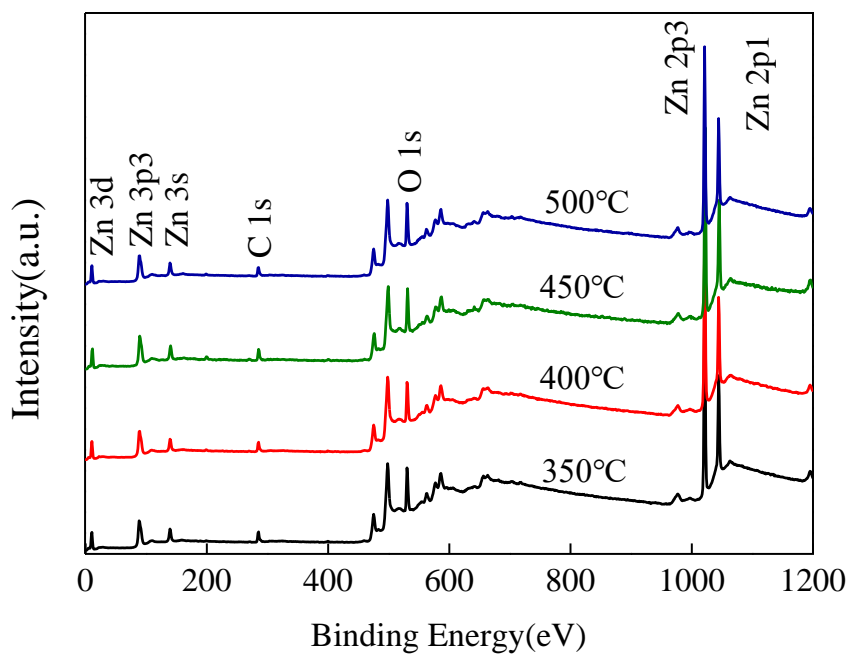


**Figure 5.** ESR spectra of ZnO films under different annealing temperatures

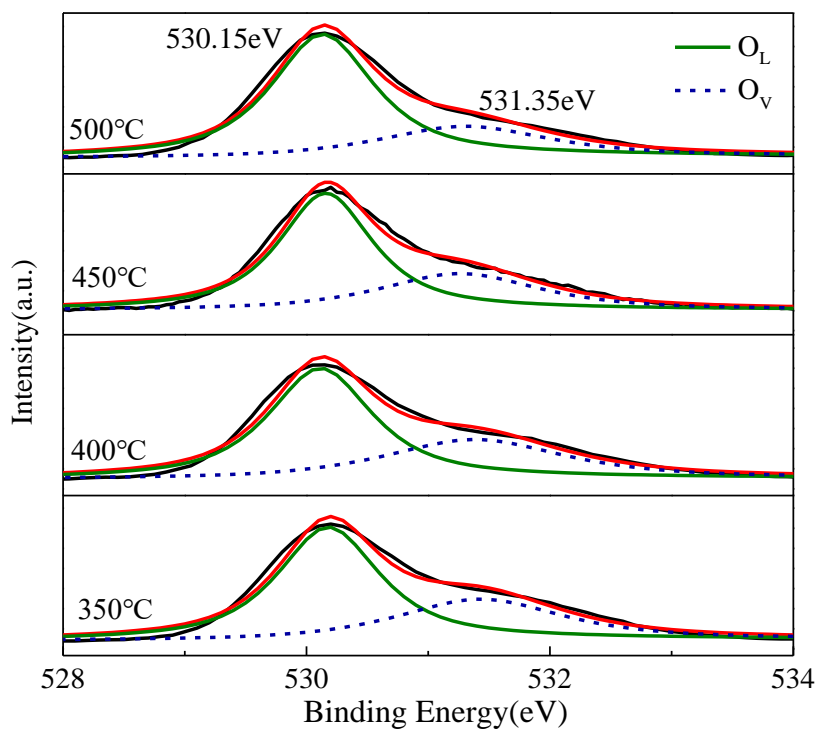
### 3.5 XPS spectrum

Fig. 6 shows the XPS survey spectrum and high-resolution spectra of ZnO films under different annealing temperatures. In the survey spectrum, Zn and O were observed in the ZnO films (Fig. 6a), which is consistent with the EDS result in Fig. 2. In the high-resolution spectrum of O1 s, two peaks existed, where the peak at a binding energy of 530.15 eV was related to the oxygen atom in the ZnO lattice ( $O_L$ ) and the peak at a binding energy of 531.35 eV was related to the oxygen vacancies in the ZnO film ( $O_V$ ) [28, 29].

By analysing the areas of peaks at 530.15 eV ( $O_L$ ) and 531.35 eV ( $O_V$ ) [30], the contents of  $O_L$  and  $O_V$  in ZnO films were calculated, and they are listed in Table 2. With increasing annealing temperature, the content of oxygen vacancies ( $O_V$ ) in the ZnO film gradually increased from 33.94% (350°C) to 36.88% (400°C), 37.12% (450°C) and 40.31% (500°C), which coincides with the EDS and ESR results in Fig. 2 and Fig. 5.



(a) Survey spectrum



(b) O1 s region

**Figure 6.** XPS spectra of ZnO films under different annealing temperatures

**Table 2.** Binding energy and valance state of oxygen for the O1 s spectrum

Annealing temperature (°C)	Binding Energy (eV)	Valance state of oxygen	The content of oxygen in different states (%)
350	530.15	O <sub>L</sub>	66.06
	531.35	O <sub>V</sub>	33.94
400	530.15	O <sub>L</sub>	63.12
	531.35	O <sub>V</sub>	36.88
450	530.15	O <sub>L</sub>	62.98
	531.35	O <sub>V</sub>	37.12
500	530.15	O <sub>L</sub>	59.69
	531.35	O <sub>V</sub>	40.31

### 3.6 Mott-Schottky curve

The Mott-Schottky curves of ZnO films under different annealing temperatures are shown in Fig. 7. In the potential range from -0.2 V to 0.8 V, the Mott-Schottky curve of the ZnO film has a positive slope, which indicates that the prepared ZnO film is an *n*-type semiconductor and that the carrier ion in ZnO films is an oxygen vacancy.

After calculation by equation (1), the slope of the Mott-Schottky curve and oxygen vacancy concentration in the ZnO film were calculated, and they are listed in Table 3. It can be seen from Table 3 that the oxygen vacancy concentration  $N_D$  in the ZnO film is clearly increased from  $4.077 \times 10^{20} \text{ cm}^{-3}$  (350°C) to  $1.237 \times 10^{21} \text{ cm}^{-3}$  (400°C),  $1.356 \times 10^{21} \text{ cm}^{-3}$  (450°C) and  $7.018 \times 10^{21} \text{ cm}^{-3}$  (500°C) with the increasing annealing temperature, which is also consistent with the EDS, ESR and XPS results in Fig. 2, Fig. 5, Fig. 6 and Table 2.

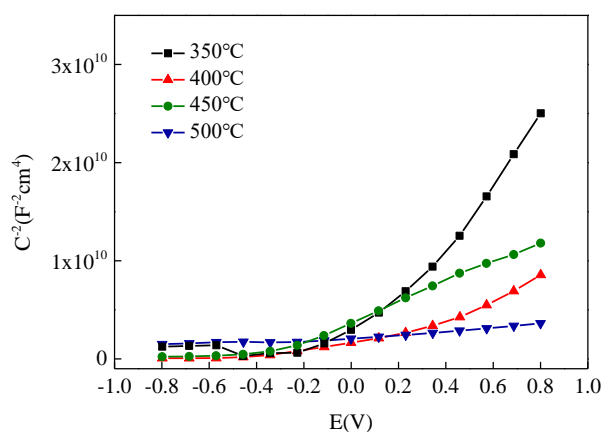


**Figure 7.** Mott-Schottky curves of ZnO films under different annealing temperatures in a 3.5 wt % NaCl solution

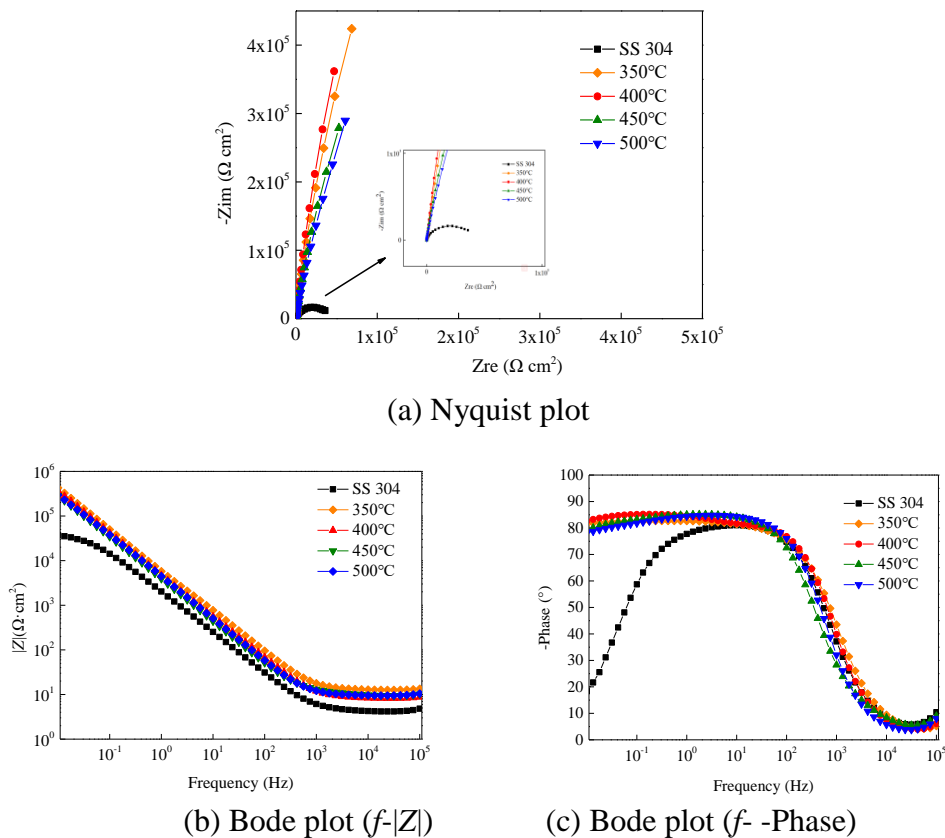
**Table 3.** Carrier density ( $N_D$ ) in ZnO films under different annealing temperatures

Temperatures (°C)	Slope ( $\text{cm}^4 \cdot \text{F}^{-2} \cdot \text{V}^{-1}$ )	$N_D$ ( $\text{cm}^{-3}$ )
350	$3.46 \times 10^{10}$	$0.407 \times 10^{21}$
400	$1.14 \times 10^{10}$	$1.237 \times 10^{21}$
450	$1.03 \times 10^{10}$	$1.356 \times 10^{21}$
500	$0.20 \times 10^{10}$	$7.018 \times 10^{21}$

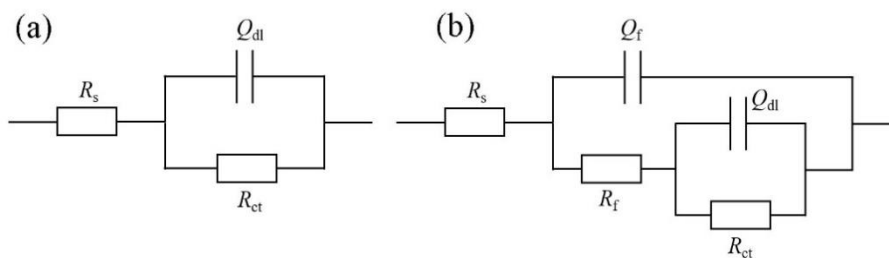
### 3.7 EIS spectrum

Fig. 8 shows the EIS spectrum of the ZnO film under different annealing temperatures in a 3.5 wt % NaCl solution. In the EIS spectrum of the 304 steel substrates, one capacitance arc was observed with an impedance modulus of 0.01 Hz of  $3.5 \times 10^4 \Omega \cdot \text{cm}^2$ . After the ZnO film formed on the steel substrate, two capacitance arcs were observed (Fig. 8a). Whereas the capacitance arc at high frequency was caused by the resistance and capacitance of the ZnO film, the capacitance arc at low frequency was related to the charge transfer resistance and double layer capacitance of the steel substrate [31]. In the middle and low frequency ranges of the Bode plots (Fig. 8b and Fig. 8c), the slope of the  $f-|Z|$  curve is close to -1, and the phase angle is close to  $-90^\circ$ , which indicates that the prepared ZnO film has good capacitance characteristics [9]. With increasing annealing temperature, the impedance modulus of the ZnO film at 0.01 Hz first increased from  $4.29 \times 10^5 \Omega \cdot \text{cm}^2$  (350°C) to  $3.64 \times 10^5 \Omega \cdot \text{cm}^2$  (400°C) and then decreased from  $2.95 \times 10^5 \Omega \cdot \text{cm}^2$  (450°C) to  $2.83 \times 10^5 \Omega \cdot \text{cm}^2$  (500°C). However, the impedance modulus of the ZnO film is approximately ten times the corresponding modulus of the 304 steel substrate, which proves that the ZnO film has a better protection effect for 304 steel.

For the above EIS spectrum in Fig. 8, the equivalent circuit in Fig. 9 is applied, in which  $R_s$ ,  $R_f$ , and  $R_{ct}$  are the solution resistance, film resistance and charge transfer resistance, respectively, whereas  $Q_f$  and  $Q_{dl}$  are the film capacitance and electric double layer capacitance, respectively. The calculated electrochemical parameters are listed in Table 4. The charge transfer resistance of the 304 steel substrate is only  $4.95 \times 10^4 \Omega \cdot \text{cm}^2$  in a 3.5 wt% NaCl solution. After the formation of the ZnO film on the steel substrate, the charge transfer resistance  $R_{ct}$  is increased to the range  $1.18 \times 10^6 \Omega \cdot \text{cm}^2$ - $1.02 \times 10^7 \Omega \cdot \text{cm}^2$  with a protection efficiency of 95.80%-99.51%. As the annealing temperature increases, the  $R_{ct}$  and protection efficiency of the ZnO film first increases and then decreases. Among these four annealing temperatures, the ZnO film prepared at 400°C has the highest  $R_{ct}$  value of  $1.02 \times 10^7 \Omega \cdot \text{cm}^2$  and the best protection efficiency of 99.51%.



**Figure 8.** EIS spectrum of a 304 SS substrate and ZnO films in a 3.5 wt % NaCl solution



**Figure 9.** Equivalent electrical circuit used for the EIS spectrum

**Table 4.** Fitting electrochemical parameters for the EIS spectrum of a 304 SS substrate and ZnO films in a 3.5 wt % NaCl solution

Sample	$R_s$ ( $\Omega \cdot \text{cm}^2$ )	$Q_f$ ( $\mu\Omega^{-1} \cdot \text{cm}^{-2} \cdot \text{S}^{n_f}$ )	$n_f$	$R_f$ ( $\Omega \cdot \text{cm}^2$ )	$Q_{dl}$ ( $\mu\Omega^{-1} \cdot \text{cm}^{-2} \cdot \text{S}^{n_{dl}}$ )	$n_{dl}$	$R_{ct}$ ( $\Omega \cdot \text{cm}^2$ )	$\eta$ (%)
SS304	6.69				$4.29 \times 10^{-5}$	0.96	$4.95 \times 10^4$	
350°C	12.77	$2.66 \times 10^{-5}$	0.93	$4.11 \times 10^3$	$4.98 \times 10^{-6}$	1.00	$6.69 \times 10^6$	99.26
400°C	8.30	$3.48 \times 10^{-5}$	0.94	$3.97 \times 10^3$	$7.61 \times 10^{-6}$	1.00	$1.02 \times 10^7$	99.51
450°C	10.31	$1.14 \times 10^{-5}$	0.71	$3.12 \times 10^3$	$3.53 \times 10^{-5}$	0.96	$5.84 \times 10^6$	99.15
500°C	9.45	$2.04 \times 10^{-5}$	1.00	$2.99 \times 10^3$	$4.11 \times 10^{-5}$	0.94	$1.18 \times 10^6$	95.80

3.8 Immersion behaviour

Fig. 10 shows the surface morphology of the ZnO film before immersion and during immersion in a 3.5 wt % NaCl solution for 16 h. Before this immersion, the ZnO films had a smooth and compact surface (Fig. 10a). Although many pores formed on the surface of the film after the immersion, no corrosion products were observed (Fig. 10b).

The element composition and O/Zn ratio of the ZnO film before and after the immersion test are shown in Table 5. The ratio of O/Zn of the ZnO film after the immersion test (0.75) is larger than the same ratio before the immersion (0.68), which means that the oxygen content in the ZnO film gradually increased with a prolonged immersion.

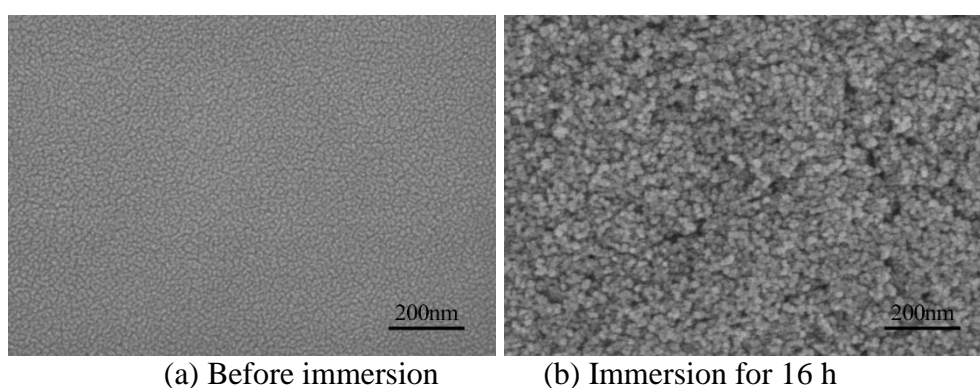


**Figure 10.** Surface morphology of ZnO films annealed at 400°C before and after immersion (×100000)

**Table 5.** Element composition and O/Zn ratio of a ZnO film annealed at 400°C before and after immersion

Immersion time (h)	Relative content (%)		O/Zn
	Zn	O	
0	21.13	14.36	0.68
16	12.08	9.12	0.75

The O1 s spectrum of the ZnO film before and after immersion in a 3.5 wt % NaCl solution is shown in Fig. 11, and the contents of the two oxygen states are given in Table 6. In the O1 s spectrum, two peaks at 530.15 eV and 531.35 eV are observed, which represent lattice oxygen and oxygen vacancies, respectively, as shown in Fig. 6. Before immersion, the content of the oxygen vacancies was approximately 36.41%. However, the content of the oxygen vacancies was reduced to 35.23% after the immersion test, which is consistent with the O/Zn ratio of the ZnO film in Table 5.

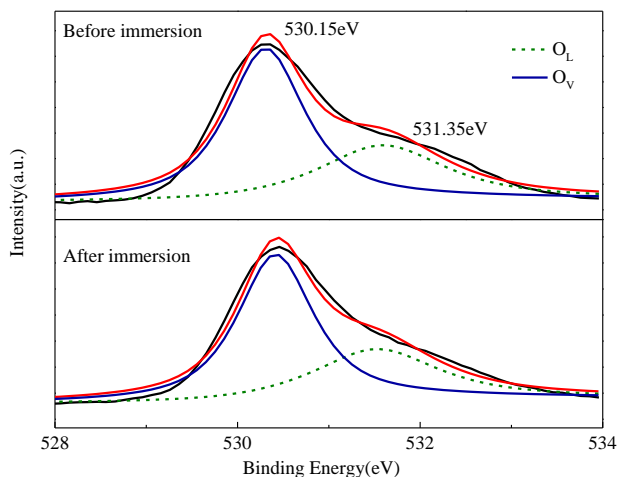


**Figure 11.** XPS spectrum of O1 s in ZnO film before and after immersion in a 3.5 wt % NaCl solution

**Table 6.** Binding energy and relative content of oxygen from the O1 s spectrum for the ZnO film before and after immersion

Immersion time (h)	Binding Energy (eV)	Valance state of oxygen	Relative content (%)
0	530.15	O <sub>L</sub>	63.59
	531.35	O <sub>V</sub>	36.41
16	530.15	O <sub>L</sub>	64.77
	531.35	O <sub>V</sub>	35.23

The Mott-Schottky curves of the ZnO film during the immersion process in a 3.5 wt % NaCl solution are shown in Fig. 12. In the potential range from -0.2 V to 0.6 V, the ZnO film has a positive slope throughout the immersion process, which means that the carrier ion in ZnO films is still an oxygen vacancy. After calculation, the concentration of the oxygen vacancies in the ZnO film is shown in Fig. 13. With a prolonged immersion time, the concentration of oxygen vacancies in the ZnO film obviously decreased from the initial  $3.289 \times 10^{21} \text{ cm}^{-3}$  to the final  $3.685 \times 10^{20} \text{ cm}^{-3}$ , which coincides with the EDS and XPS results in Table 5 and Table 6.

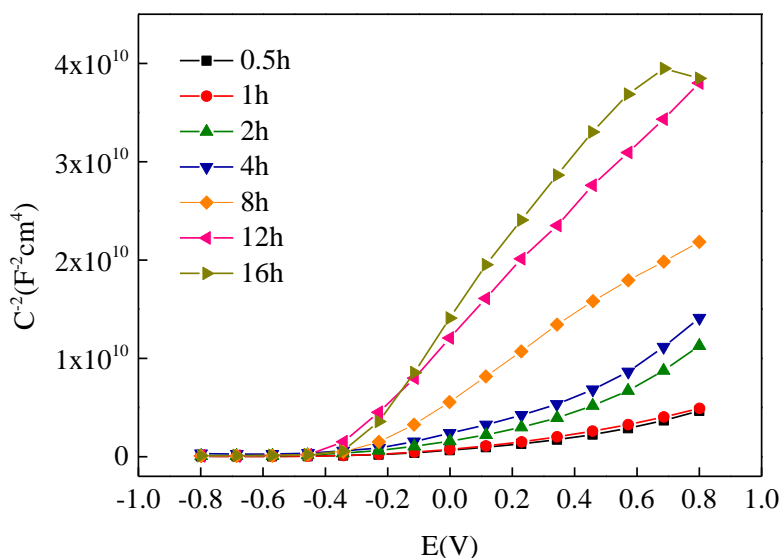


**Figure 12.** Mott-Schottky curves of a ZnO film during the immersion process in a 3.5 wt % NaCl solution

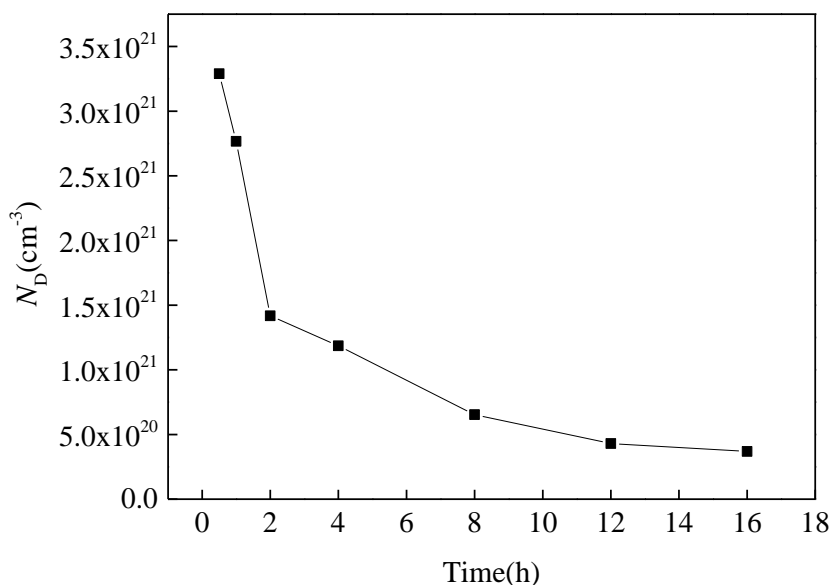


**Figure 13.** Oxygen vacancy concentration of a ZnO film during the immersion process

Fig. 14 shows the EIS spectrum of the ZnO film at different immersion times in a 3.5 wt% NaCl solution. During the immersion process, in the EIS spectrum, two capacitance arcs were observed (Fig. 14a, Fig. 14c). In the middle and low frequency ranges, the slope of  $f-|Z|$  was close to -1, and the phase angle was close to  $-90^\circ$  (Fig. 14b, Fig. 14c). All of these results prove that during the immersion process, the ZnO film had good capacitance characteristics with higher corrosion resistance.

By analysing the equivalent circuit in Fig. 9, the electrochemical parameters for the EIS spectrum in Fig. 13 were calculated, and they are listed in Table 7. It can be deduced from Table 7 that

both the film resistance  $R_f$  and the charge transfer resistance  $R_{ct}$  of the ZnO film continuously increase with prolonged immersion time, which indicates that the protective performance of ZnO films was improved with the immersion process.

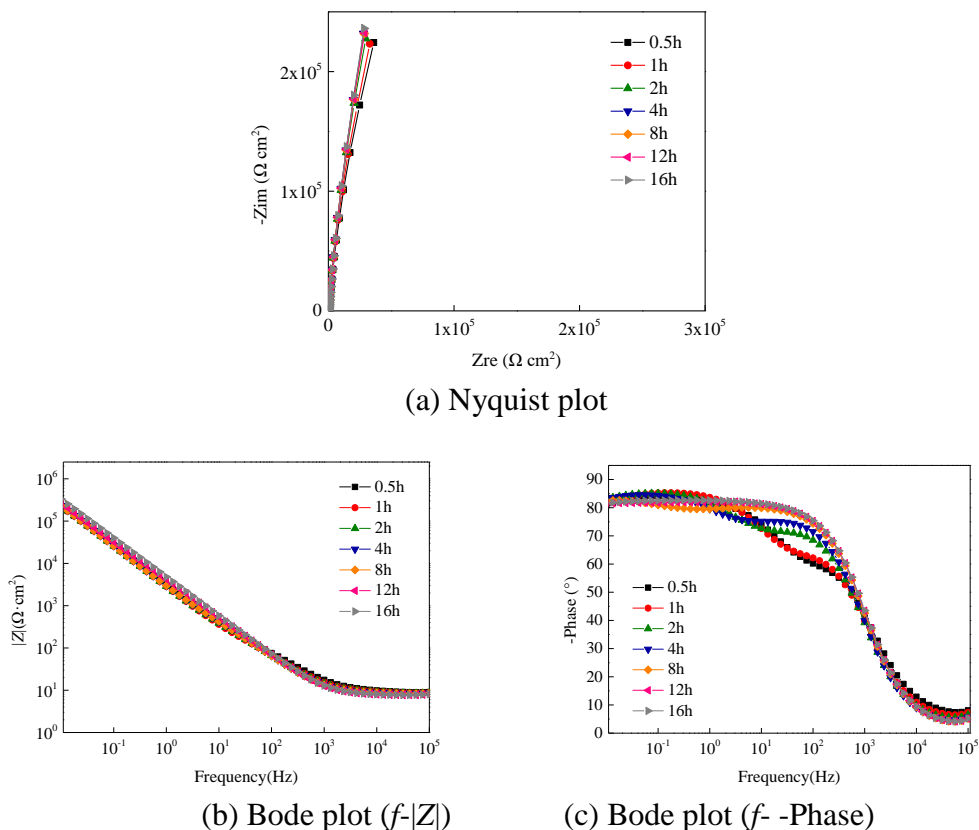


**Figure 14.** EIS spectrum of a ZnO film at different immersion times in a 3.5 wt % NaCl solution

**Table 7.** Fitting electrochemical parameters for the EIS spectrum of a ZnO film at different immersion times in a 3.5 wt % NaCl solution

Time (h)	$R_s$ ( $\Omega \cdot \text{cm}^2$ )	$Q_f$ ( $\mu\Omega^{-1} \text{cm}^{-2} \text{S}^{n_f}$ )	$n_f$	$R_f$ ( $\Omega \cdot \text{cm}^2$ )	$Q_{dl}$ ( $\mu\Omega^{-1} \text{cm}^{-2} \text{S}^{n_{dl}}$ )	$n_{dl}$	$R_{ct}$ ( $\Omega \cdot \text{cm}^2$ )
0.5	9.31	$3.56 \times 10^{-5}$	0.88	$0.19 \times 10^3$	$2.19 \times 10^{-5}$	0.96	$2.532 \times 10^6$
1	9.05	$4.08 \times 10^{-5}$	0.89	$1.76 \times 10^3$	$2.08 \times 10^{-5}$	0.99	$7.356 \times 10^6$
2	8.86	$4.21 \times 10^{-5}$	0.90	$2.48 \times 10^3$	$1.79 \times 10^{-5}$	1.00	$1.502 \times 10^7$
4	8.47	$4.47 \times 10^{-5}$	0.90	$3.14 \times 10^3$	$1.39 \times 10^{-5}$	1.00	$7.295 \times 10^7$
8	8.18	$4.58 \times 10^{-5}$	0.90	$5.53 \times 10^3$	$1.09 \times 10^{-5}$	1.00	$2.687 \times 10^8$
12	7.75	$4.49 \times 10^{-5}$	0.89	$6.39 \times 10^3$	$9.68 \times 10^{-6}$	1.00	$2.769 \times 10^8$
16	7.55	$2.71 \times 10^{-5}$	0.91	$6.09 \times 10^3$	$1.33 \times 10^{-5}$	1.00	$2.872 \times 10^8$

### 3.9 Resistive switching performance

Fig. 15 shows the EIS spectrum of the ZnO film during the resistive switching process. In this process, I-0.5, II-0.5 and III-0.5 were labelled ZnO films in the initial preparation and after each immersion-polarization process, and 4.0, I-4.0, II-4.0 and III-4.0 represent the above samples after 4.0

hours of immersion in a 3.5% NaCl solution. During the resistive switching process, two capacitance arcs were still observed in the EIS spectrum (Fig. 15a, Fig. 15c). The slope of  $f^{-1}|Z|$  is close to -1, and the phase angle is close to  $-90^\circ$  in the middle and low frequency ranges (Fig. 15, Fig. 15c). These results imply that during the resistive switching process, the ZnO film still has good capacitance characteristics with a higher corrosion resistance.

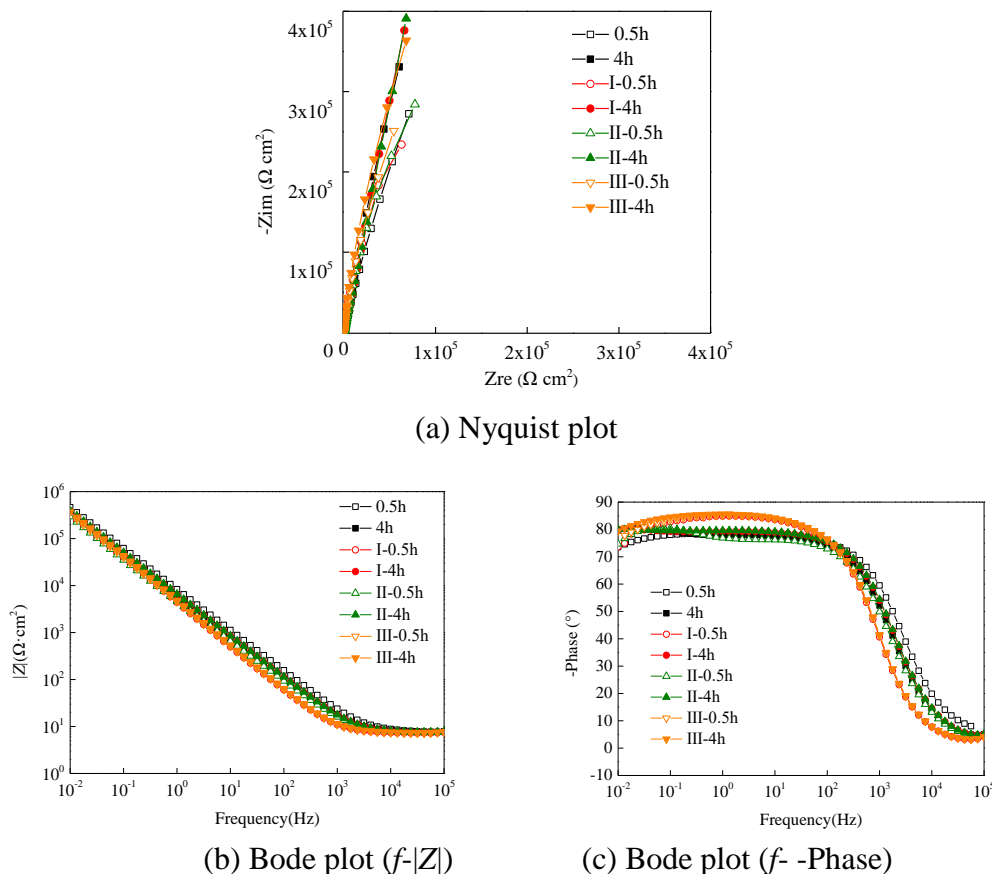


**Figure 15.** EIS spectrum of a ZnO film in a 3.5 wt % NaCl solution during the resistive switching process

**Table 8.** Fitting electrochemical parameters for a ZnO film in a 3.5 wt % NaCl solution during the resistive switching process

Time (h)	$R_s$ ( $\Omega \cdot \text{cm}^2$ )	$Q_f$ ( $\mu\Omega^{-1} \cdot \text{cm}^{-2} \cdot \text{S}^{nf}$ )	$n_f$	$R_f$ ( $\Omega \cdot \text{cm}^2$ )	$Q_{dl}$ ( $\mu\Omega^{-1} \cdot \text{cm}^{-2} \cdot \text{S}^{ndl}$ )	$n_{dl}$	$R_{ct}$ ( $\Omega \cdot \text{cm}^2$ )
0.5	5.83	$1.93 \times 10^{-6}$	0.88	$0.23 \times 10^3$	$2.21 \times 10^{-5}$	0.87	$6.21 \times 10^6$
4.0	7.89	$1.32 \times 10^{-6}$	1.00	$2.75 \times 10^3$	$3.61 \times 10^{-5}$	0.87	$4.49 \times 10^7$
I-0.5	7.28	$3.41 \times 10^{-5}$	0.94	$1.06 \times 10^3$	$6.32 \times 10^{-6}$	0.91	$1.44 \times 10^6$
I-4.0	7.13	$1.34 \times 10^{-6}$	1.00	$2.75 \times 10^3$	$3.09 \times 10^{-5}$	0.88	$2.83 \times 10^8$
II-0.5	7.61	$3.96 \times 10^{-5}$	0.87	$1.29 \times 10^3$	$3.30 \times 10^{-6}$	1.00	$1.77 \times 10^6$
II-4.0	8.25	$1.42 \times 10^{-4}$	1.00	$2.47 \times 10^3$	$2.98 \times 10^{-5}$	0.88	$1.62 \times 10^8$
III-0.5	7.27	$3.35 \times 10^{-5}$	0.95	$1.64 \times 10^3$	$5.48 \times 10^{-6}$	0.93	$2.56 \times 10^6$
III-4.0	7.49	$3.06 \times 10^{-5}$	0.951	$2.82 \times 10^3$	$5.49 \times 10^{-6}$	0.936	$2.13 \times 10^8$

By applying the equivalent circuit in Fig. 9, the electrochemical parameters for the EIS spectrum in Fig. 15 are calculated and listed in Table 8. From Table 8, it can be seen that ZnO film in the as-prepared state and after polarization treatment has a lower film resistance  $R_f$  and charge transfer resistance  $R_{ct}$ . After the immersion test in a 3.5% NaCl solution, both the film resistance  $R_f$  and the charge transfer resistance  $R_{ct}$  of the ZnO film increased. These results prove that the resistive switching performance of the ZnO film could be fulfilled by immersion and polarization treatment.

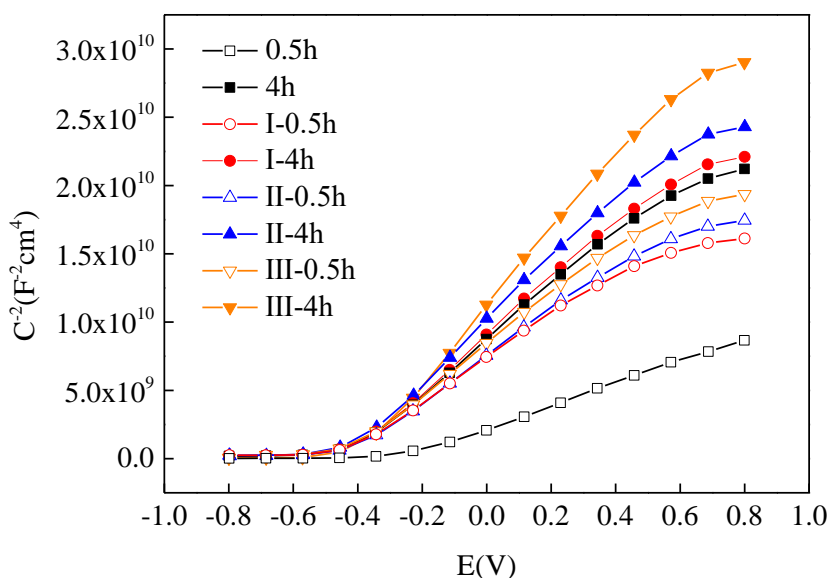


**Figure 16.** Motte-Schottky curves of a ZnO film in a 3.5 wt % NaCl solution during the resistive switching process

**Table 9.** Carrier density ( $N_D$ ) in a ZnO film during the resistive switching process

Time (h)	Slope ( $\text{cm}^4 \cdot \text{F}^{-2} \cdot \text{V}^{-1}$ )	$N_d$ ( $\text{cm}^{-3}$ )
0.5	$0.826 \times 10^{10}$	$1.690 \times 10^{21}$
4.0	$1.888 \times 10^{10}$	$0.740 \times 10^{21}$
I-0.5	$1.392 \times 10^{10}$	$1.003 \times 10^{21}$
I-4.0	$1.975 \times 10^{10}$	$0.707 \times 10^{21}$
II-0.5	$1.539 \times 10^{10}$	$0.907 \times 10^{21}$
II-4.0	$2.149 \times 10^{10}$	$0.650 \times 10^{21}$
III-0.5	$1.677 \times 10^{10}$	$0.837 \times 10^{21}$
III-4.0	$2.704 \times 10^{10}$	$0.516 \times 10^{21}$

The Mott-Schottky curves of ZnO films during the resistive switching process are shown in Fig. 16, and the calculated oxygen vacancy concentration is listed in Table 9. The ZnO film in the as-prepared state has a higher oxygen vacancy concentration of  $1.690 \times 10^{21} \text{ cm}^{-3}$ . After the immersion test in a 3.5% NaCl solution, the oxygen vacancy concentration in the ZnO film is reduced to  $0.740 \times 10^{21} \text{ cm}^{-3}$ . By applying the polarization treatment, the oxygen vacancy concentration in the above corroded ZnO film was increased to a higher value of  $1.003 \times 10^{21} \text{ cm}^{-3}$ , which almost indicates restoration to the

concentration in the as-prepared state. In the following immersion and polarization process, the oxygen vacancy in the ZnO film switched between higher and lower concentrations and slightly decreased with increasing process time. All of these results show that the resistive switching performance of the ZnO film could be obtained by the immersion and polarization treatment.

## 4. DISCUSSION

### 4.1 Effect of annealing temperature

From the above experimental results, as the annealing temperature gradually increased from 350°C to 500°C, whereas the crystal structure of the ZnO film remained stable, the grain size of the ZnO increased (Fig. 1, Fig. 2 and Table 1) and the surface of the films became smoother. In the process of increasing the annealing temperature, the value of O/Zn gradually decreased (Fig. 2e). This behaviour is consistent with the XPS, ESR and Mott-Schottky curves, which indicate that the content of oxygen vacancies in the ZnO films increased. According to crystal defect theory, the generation probability of defects such as oxygen vacancies can be expressed by the following equation [32]:

$$p = \exp \left[ - \left( \frac{E_a}{KT} \right) \right] \quad (3)$$

where  $p$  is the generation probability of the defects,  $E_a$  is the formation energy of the defect,  $K$  is the Boltzmann constant, and  $T$  is the ambient temperature of crystallization.

To explore the relationship between the annealing temperature and the oxygen vacancy content, formula (3) is used to correlate the oxygen vacancy content with the temperature, as shown in Fig. 17. Furthermore, the formation energy of oxygen vacancies is calculated (0.466 eV). Because this energy is consistent with related reports [33], it is clear that the annealing temperature will affect the oxygen vacancy content.

Due to the vacancy conduction mechanism, as the oxygen vacancy content increases, the conductivity increases and the corrosion resistance decreases. Therefore, as the annealing temperature increases, the corrosion resistance of the ZnO film decreases. However, the corrosion resistance of the film annealed at 300°C is lower than that of the film annealed at 400°C. This discrepancy occurs because the compactness of the film annealed at 300°C is lower and there are many pores on the surface that accelerate the diffusion of the corrosive medium to the substrate.

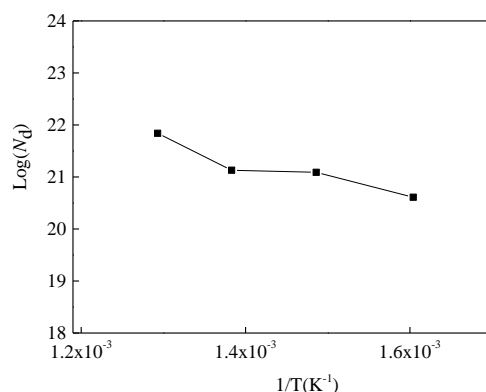


**Figure 17.** Correlation between the oxygen vacancy concentration and the annealing temperature

#### 4.2 Protection mechanism

The ZnO film has a uniform and dense surface, which can prevent the corrosive medium from reaching the substrate (Fig. 10). However, the oxygen vacancies of the ZnO film can adsorb the  $O_2$  molecules in the solution to prevent oxygen from reaching the substrate. Fig. 18 is a schematic diagram of the protection mechanism of the ZnO film. As shown in Fig. 18a, when the film is immersed in the solution, the surface of the film will adsorb  $O_2$  molecules in the solution to form chemisorbed  $O_{2(ad)}^-$  [32]. As shown in Fig. 18b and Fig. 18c,  $O_{2(ad)}^-$  will be captured and combined by the oxygen vacancies in the film during the diffusion process into the film. This process reduces the transmission of oxygen to the steel substrate and the conductivity of the film; thus, the corrosion resistance of the ZnO films is improved (see Fig. 11, Fig. 12, and Fig. 13 as well as Table 5, Table 6, and Table 7).

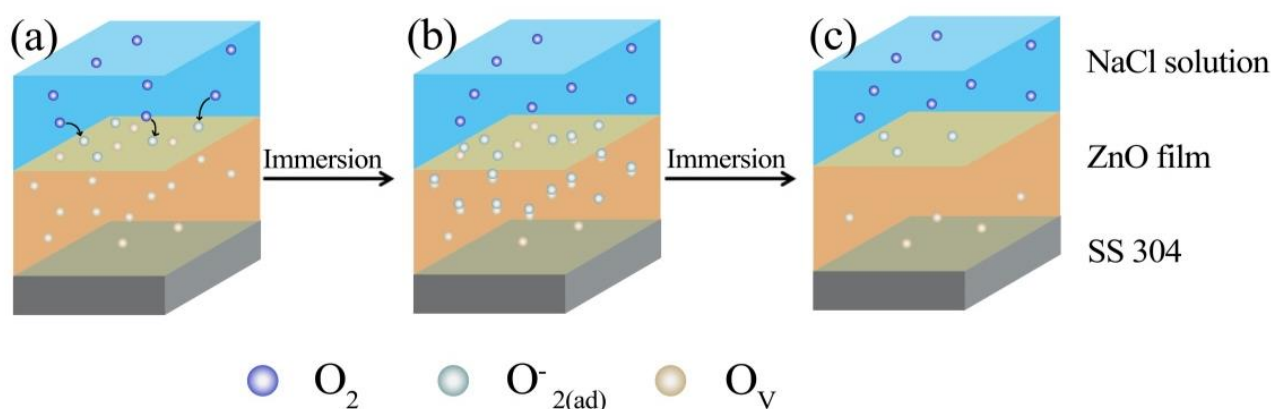


**Figure 18.** Schematic diagram of the protection mechanism of the ZnO film we employed: (a) the initial state of the ZnO film in an NaCl solution, (b) immersion in an NaCl solution for 0.5 hours, (c) immersion in an NaCl solution for 4 hours

#### 4.3 Resistive switching mechanism

For the newly prepared ZnO film, whereas the initial oxygen vacancy content is high, the resistance is low. Fig. 19 shows the resistance switching mechanism of the ZnO film. As shown in Fig. 19a, Fig. 19b and Fig. 19c, during the immersion process, the oxygen vacancies combine with the oxygen in the solution, the oxygen vacancy content of the film decreases, and the resistance increases. Therefore, the film changes to a high resistance state. However, an immersion time that is too long will deplete the oxygen vacancies in the film and cause oxygen to diffuse to the steel surface, which will cause corrosion of the steel.

As shown in Fig. 19d and Fig. 19e, to maintain good corrosion performance in the ZnO film, the ZnO film is polarized after immersion for a certain period of time. During the polarization process, the oxygen atoms in ZnO escape from the film into the solution. Moreover, because oxygen vacancies

are also generated again, the film is transformed into a state of low resistance. In the additional immersion process, the oxygen vacancies in the film can combine with the oxygen in the solution again, which will improve the corrosion resistance of the film. Such repeated immersion-polarization treatments can switch the film between high and low resistance states and prolong the service life of the film.

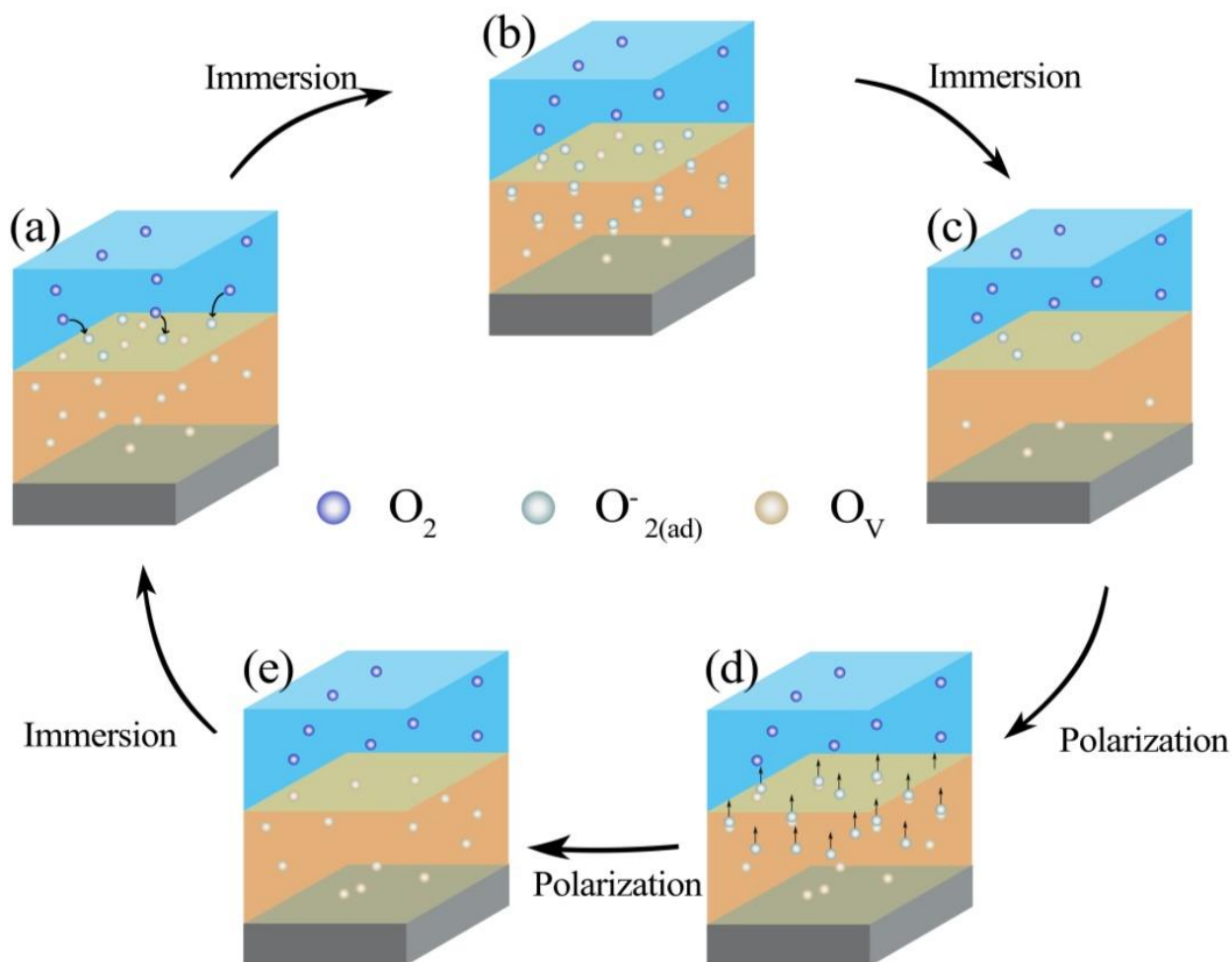


**Figure 19.** Schematic diagram of the resistance switching mechanism for the ZnO film

## 5. CONCLUSION

(1) A ZnO resistive switching film was successfully prepared on a steel surface by using the sol-gel method. The prepared ZnO film has a compact and smooth surface with an *n*-type semiconductor.

(2) With increasing annealing temperature, the ZnO film gains a lower O/Zn ratio and a higher oxygen vacancy concentration.

(3) With increasing annealing temperature, the corrosion resistance of the ZnO film first increased and then decreased. The largest corrosion resistance occurred at an annealing temperature of 400°C.

(4) By applying a negative polarization treatment, the concentration of oxygen vacancies and corrosion resistance of the film could be restored to its original state. Furthermore, the corrosion resistance of the film could be improved with a prolonged immersion time due to the combination of oxygen vacancies in the film with oxygen atoms in the solution.

#### ACKNOWLEDGEMENT

This work was supported by National Natural Science Foundation of China (No. 51771133).

#### References

1. S R Kiahosseini, A Aminian. *Bulletin of Materials Science*, 42(2019)160.
2. M Wang, J Wang, W Hu. *Progress in Organic Coatings*, 139(2020)105434.
3. Y He, G Li, K H Hwang, Y Boluk, P M Claesson. *Applied Surface Science*, 537(2021)147789.
4. T H Mekonnen, T Haile, M Ly. *Applied Surface Science*, 540(2021)148299.
5. G Batis, P Pantazopoulou, A Routoulas. *Anti-Corrosion Methods and Materials*, 48(2001)107.
6. D P Norton, Y W Heo, M P Ivill, K Ip, S J Pearton, M F Chisholm, T Steiner. *Materials Today*, 7(2004)34.
7. H Tampo, H Shibata, K Matsubara, A Yamada, P Fons, S Niki, M Yamagata, H Kanie. *Applied Physics Letters*, 89(2006)132113.
8. K Kamburova, N Boshkova, N Boshkov, T Radeva. *Colloids and Surfaces A: Physicochemical and Engineering Aspects*, 609(2021)125741.
9. J Y Wang, C M Liu, W K Chen, Y M Liu, M D Ger. *Materials Transactions*, 49(2008)1355.
10. V P M Shajudheen, S S Kumar, V S Kumar, A U Maheswari, M Sivakumar, S R Mohan. *AIMS Materials Science*, 5(2018)932.
11. J Karbowniczek, L Cordero-Arias, S Virtanen, S K Misra, E Valsami-Jones, L Tuchscher, B Rutkowski, K Górecki, P Bała, A Czyska-Filemonowicz, A R Boccaccini. *Materials Science and Engineering C*, 77(2017)780.
12. T Ramkumar, M Selvakumar, M Mohanraj, P Chandramohan, P Narayanasamy. *Journal of Materials Engineering and Performance*, 29(2020)5796.
13. D E Motaung, P R Makgwane, S S Ray. *Materials Letters*, 139(2015)475.
14. R Waser, R Dittmann, C Staikov, K Szot. *Advanced Materials*, 21(2009)2632.
15. U Chand, C Y Huang, J H Jieng, W Y Jang, C H Lin, T Y Tseng. *Applied Physics Letters*, 106(2015)153502.
16. O Lupan, T Pauporté, L Chow, B Viana, F Pellé, L K Ono, B Roldan Cuenya, H Heinrich. *Applied Surface Science*, 256(2010)1895.
17. E M C Fortunato, P M C Barquinha, A C M B G Pimentel, A M F Gonçalves, A J S Marques, L M N Pereira, R F P Martins. *Advanced Materials*, 17(2005)590.
18. Y Sun, J H Seo, C J Takacs, J Seifert, A J Heeger. *Advanced Materials*, 23(2011)1679.
19. M Ohyama, H Kozuka, T Yoko. *Thin Solid Films*, 306(1997)78.
20. M Vishwas, K N Rao, A R Phani, K V A Gowda, R P S Chakradhar. *Journal of Materials Science: Materials in Electronics*, 22(2011)1415.
21. S Zhang, R Shi, Y Tan. *Journal of Alloys and Compounds*, 711(2017)155.

22. D Raoufi, T Raoufi. *Applied Surface Science*, 255(2009)5812.
23. X Sui, Y Liu, C Shao, Y Liu, C Xu. *Chemical Physics Letters*, 424(2006)340.
24. R Subbiah, S Muthukumaran, V Raja. *Journal of Materials Science: Materials in Electronics*, 30(2019)17066.
25. M Sharma, P Jeevanandam. *Superlattices and Microstructures*, 52(2012)1083.
26. M Ashokkumar, S Muthukumaran. *Powder Technology*, 258(2014)157.
27. S M Evans, N C Giles, L E Halliburton, L A Kappers. *Journal of Applied Physics*, 103(2008)043714.
28. Y S Rim, D L Kim, W H Jeong, H J Kim. *Applied Physics Letters*, 97(2010)233502.
29. J Singh, S Juneja, S Palsaniya, A K Manna, R K Soni, J Bhattacharya. *Colloids and Surfaces B: Biointerfaces*, 184(2019)110541
30. J Wang, R Chen, L Xiang, S Komarneni. *Ceramics International*, 44(2018)7357.
31. C Liu, Q Bi, A Leyland, A Matthews. *Corrosion Science*, 45(2003)1243.
32. J J Ke, Z J Liu, C F Kang, S J Lin, J H He. *Applied Physics Letters*, 99(2011)192106
33. R Dutta, N Mandal. *Applied Physics Letters*, 101(2012)042106.

© 2021 The Authors. Published by ESG ([www.electrochemsci.org](http://www.electrochemsci.org)). This article is an open access article distributed under the terms and conditions of the Creative Commons Attribution license (<http://creativecommons.org/licenses/by/4.0/>).